Biomedical Physics & Engineering Express

Endorsed by IPEM Institute of Physics and Engineering in Medicine

ACCEPTED MANUSCRIPT

Assessment of PTV margin adequacy for single isocenter multiple brain metastases using genetic algorithms

To cite this article before publication: José Alejandro Rojas López *et al* 2023 *Biomed. Phys. Eng. Express* in press https://doi.org/10.1088/2057-1976/acdde5

Assessment of PTV margin adequacy for single isocenter multiple brain metastases using genetic algorithms

Rojas-López, José Alejandro[1,2,a], Venencia, Carlos Daniel[3,b], Chesta, Miguel Ángel[1,c], Tamarit, Francisco[1,d]

[1]Universidad Nacional de Córdoba, X5000HUA, Av. Medina Allende, Córdoba, Argentina
[2]Hospital Almater, 21100, Av. Francisco I. Madero 1060, Mexicali, Baja California, México
[3]Instituto Zunino, X5000BFI, Obispo Oro 423, Córdoba, Argentina

[a]alexrojas@ciencias.unam.mx
[b]dvenencia@institutozunino.org
[c]miguel.chesta@unc.edu.ar
[d]francisco.tamarit@unc.edu.ar

Abstract

Purpose: To study the impact on dose coverage and the dose to the healthy tissue applying optimized margins in single isocenter multiple brain metastases radiosurgery (SIMM-SRS) in linac machine based on setup rotations/translations induced errors calculated by a genetic algorithm (GA).
Method: The following quality indices of SIMM-SRS were analyzed for 32 plans (256 lesions): Paddick conformity index (PCI), gradient index (GI), maximum (D_{max}) and mean (D_{mean}) doses, local and global V_{12} for the healthy brain. A GA based on Python packages were used to determine the maximum shift produced by induced errors of 0.2º/0.2 mm, and 0.5º/0.5 mm in 6 degrees of freedom.
Results: In terms of D_{max}, and D_{mean}, the quality of the optimized-margin plans remains unchanged ($p>0.072$) concerning the original plan. However, considering the 0.5º/0.5 mm plans, PCI and GI decreased for ≥ 10 metastases, and local, and global V_{12} increased considerably in all cases. To consider 0.2º/0.2 mm plans, PCI and GI get worse but local, and global V_{12} improved in all cases.
Conclusion: GA facilities to find the individualized margins automatically among the number of possible permutations of the setup order. The user-dependent margins are avoided. This computational approach takes into account more SRS sources of uncertainty, enabling the protection of the healthy brain by "smartly" reducing the margins, and maintaining clinically acceptable target volumes' coverage in most cases.

Keywords

Genetic algorithm, radiosurgery, brain metastases, single isocenter, PTV margin.

1. Introduction

Recently, an efficient technique for radiosurgery (SRS) of multiple intracranial metastases has been used[1-2]. This technique is called single isocenter multiple metastases for stereotactic radiosurgery (SIMM-SRS) and it can be performed by dynamic arcs (DCA) or volumetric modulated arc therapy (VMAT). In particular, VMAT has better conformity and faster delivery time than DCA, but DCA had lower peripheral dose spread than VMAT[3], remaining equivalent dose conformity and dose falloff for gross tumor targets (GTVs) and reducing the dose for healthy tissue[4-8].

SRS requires high-dose delivery, high-dose gradient, and sub-millimeter precision. Thus, it is important to carefully define the sources of uncertainty[9-16] to ensure both coverage and maximize sparing. In particular, the impact of intra- and inter-fractional setup shifts

on the dose distribution has been studied for rotations and translations[17-22]. The importance of an intensive description of these sources of uncertainty allows us to have detailed information to assign proper margins to the targets that ensure the dose delivery and protect healthy tissue.

At present, the consensus[23-25] on the planning target volume (PTV) assignment is to select margin sizes about the distance to the isocenter and/or volume size. Nevertheless, a previous work[16] showed that these margins should be increased, considering 3D shifts applying rotations up to 1º. Although SRS modern setups employ an image guide that strives to minimize positioning error within the region of interest for kV/DRR (digitally reconstructed radiography) image fusion regardless of isocenter position, a careful assessment of rotational error should be carried out by each clinic taking into account their combined effect with image-guided radiotherapy (IGRT), intra- and inter-fraction uncertainties to determine corresponding treatment margins due to any possible residual rotation away from the isocenter[26,27].

Thereby it is required a more grounded criterion that takes into account more variables (not only geometric), considering that in SIMM-SRS there are intra- and inter-fraction rotations and translations in the 6 degrees of freedom (DOF). Thus, the impact of setup uncertainties produced by rotations and translations has been extensively studied[15-16] to propose tools for PTV margins based on geometric/dosimetric information. Nonetheless, these studies have only a statistical approach, or they were performed with in-house software that is not available to the clinical community. Therefore, it is convenient to provide open-source tools for the use of complex DICOM files into natural pythonic objects for easy manipulation and to illustrate their use for PTV margin assessment. In particular, it is necessary to consider that rotations are a non-commutative group of transformations, thus the rotational shift of a target is strongly dependent on the order and direction of how they are performed. Adding the combined effect of translations and rotations, the total possible combinations grow up to $6! \times 2^6 = 46080$. For that reason, the maximum induced error (roll, pitch, yaw, x, y, z) could be optimized by exhaustive methods or by metaheuristic algorithms.

There are many metaheuristics algorithms[28-32]. In this study, we have investigated the genetic algorithm (GA) because its code structure and the setup information encoding are easy to implement. The GAs are optimization techniques based on Darwinian evolution. In particular, for radiotherapy, the application of GA could improve the selection of gantry angles in a reasonable time frame for intensity-modulated plans[32]. GAs have also been successfully used to optimize the design of SRS[33]. The good acceptance of GA allows us to study the PTV margin optimization in SIMM-SRS.

This work aims to compare the impact on dose coverage and the protection of healthy tissue by applying optimized PTV margins in SIMM-SRS performed in a linac based on intra-fraction induced errors calculated by a GA. This evaluation can provide a wider criterion for assigning margins based on geometric information (distance to the isocenter and volume) as well as setup errors. The validity of using a maximum shift to create margins is based on statistical and clinical studies that report a high dosimetric impact produced by rotations[34] that could be reduced with the increase of the margins with the caveat that the dose to the healthy brain is increased[35].

2. Method and materials

2.1. Treatment unit and planning system

Elements™ Multiple Mets SRS v3.0 (Brainlab AG, Munchen, Germany) is a commercial treatment planning system (TPS) that automatically optimizes a dedicated set of DCA to

treat brain lesions by single isocenter[36]. The beams of the Elements™ plans were selected from a predefined template with 5 table angles. Both templates were defined following the institutional protocol. The isocenter was equal to the center of mass of all GTVs. The treatment machine used was a TrueBeam STx® (Varian Medical Systems, Palo Alto, CA) with a flattening filter, high-definition multileaf collimator (HDMLC), and 6 MV.

Dose calculation was performed with a 1 mm grid using the Brainlab pencil beam algorithm[37-38]. The plans were created using a dose template for a single fraction of 21 Gy with a desired PTV coverage of 99% and a tolerated coverage of 95%. The templates were set to aim for a homogeneous dose distribution within the PTV.

2.2. Ethical considerations

The Institutional Quality Committee (Comité de Calidad Institucional) from our institution approved and authorised the use of this information, the results and the ethical conduct of this study under the following considerations.

The treatment plans were selected and anonymized. There was no relationship between the plan and the personal data of the patients.

2.3. Plan selection

Thirty-one SIMM-SRS plans (256 brain metastases in total) were selected randomly and retrospectively. The average number of metastases was 8 ± 5 [2, 40] per plan with an average GTV volume of 0.6 ± 1.6 cc [0.01 cc, 14.16 cc]. The prescribed dose to PTV volume was 21 Gy to D_{99}. The quality index obtained from Elements™ report: Paddick conformity index (PCI), gradient index (GI), mean dose (D_{mean}), maximum dose (D_{max}) defined as the calculated maximum dose in the voxels are shown in Supporting Information, the dose to healthy brain (HB) were reported. The HB was defined as the volume of the whole brain (WB) minus the volumes of the GTVs and the brainstem.

The institutional PTV margin criterion followed is based on the consensus approach[23-25] briefly remarked on in the introduction. If the GTV is located less than 50 mm from the isocenter, a margin of 0.5 mm was assigned. If the GTV is located more than 50 mm from the isocenter or its volume was smaller than 0.1 cc, a margin of 1 mm was assigned.

2.4. Induced shifts

A widespread way to study the dosimetric impact due to discrepancies between the original plan and actual treatment setup is based upon the 6DOF shift simulation of the target from the set of reference images. In particular, if the shifts are relatively small concerning the relevant anatomical dimensions and the radiological path of the treatment beams toward the targets[26], it is valid to displace only the target (from the structure DICOM file), without considering the shift of the dose matrix and CT. Therefore, the shift of the structure is calculated as the module of the difference vector $d = |\overrightarrow{r_{OI}} - \overrightarrow{r_{IO'}}|$ where O is the center of mass of the original structure, O' is the center of mass of the displaced structure, and I is the isocenter.

The plans studied in this work were analyzed by inducing shifts of 0.2º/0.2 mm, and 0.5º/0.5 mm in 6DOF. These configurations of induced errors were considered based on our clinical experience, variations of 0.5º/0.5 mm were observed, for which reason it was decided to study the impact that these errors could have on a plan. In addition, 0.2º/0.2 mm was included as a lower threshold of possible errors.

The shifts were performed with Python tools. It was built a Python open-source code, that uses DICOM files to provide and manage relevant information for research and clinical staff and induced errors for establishing individual margins for intracranial lesions in SIMM-SRS[39]. For statistical analysis, Spearman's correlation coefficient was calculated on Python v.3.10 to determine the correlation between the distance to isocenter and the maximum induced error.

2.5. Optimization algorithm

The GA is one of the lines of artificial intelligence, which is inspired by Darwinian evolution and its genetic-molecular basis[40]. The GA was implemented with PyGAD package[41], using the parameters, and fitness function reported in Supporting Information. The chromosome structure is shown in Supporting Information. To compare the solutions (time and the number of generations) reached by GA, an exhaustive method was performed (see Appendix).

2.6. Intra-fraction errors

An offline analysis was performed to quantify intra-fraction errors in 6DOF. The setup values were obtained retrospectively for each beam configuration for each plan (Table 1) from ARIA® information system (Varian Medical Systems, Palo Alto, CA). The error was calculated as the relative difference between the reference and the real values.

2.7. Dosimetric evaluation

The PTV margin was assigned based on the maximum induced errors produced by rotations/translations. The plans were recalculated and the quality indices in PTVs and the monitor units (MU) were contrasted with the original plans. The dosimetric degradation was evaluated by the dosimetric differences. The relative differences in the quality indices were calculated for the original and margin-optimized plans.

In addition, one of the main predictors of necrosis is the volume of the HB that receives 12 Gy (V_{12}). The associated values with V_{12} were global or local. The definition of global and local V_{12} is as follows, based on the information reported by Brainlab[42]. The global V_{12} is the total volume within the HB that exceeds the threshold of 12 Gy. The local V_{12} is defined as the geometric overlap between the target volume and the isodose (12 Gy) dose cluster located around the target volume. If several target volumes overlap with the same dose cluster, the target volumes share the dose cluster. The volume of shared dose clusters contributes entirely to the local V_{12} of each of the target volumes it is associated with. We compared local and global V_{12} for HB and WB, and different dose levels, such as V_{10} and V_5 for the plans recalculated.

An issue specific to multiple metastases SRS is whether V_{12} is reported per lesion or per plan and whether risks of necrosis are reported per lesion or per plan[43]. In a 2020 study of single-fraction SRS in 40 patients with 10 brain metastases[44], the local V_{12} predicted risks of posttreatment changes suggestive of necrosis, as opposed to the global V_{12}. To evaluate the dosimetric impact of the decrease/increase of the margins, we differentiate the results in both cases, the plans with less than 10 brain metastases and the plans with 10 or more.

For statistical analysis, a t-test of one tail was performed with a p-value equals to 0.05 to establish statistically significant differences between the quality indices.

3. Results

The global maximum shift computed by the combination of rotations/translations is reached by the exhaustive search. This value was compared, in relative difference, with the GA solution achieved in a particular number of generations as shown in Table 1. Likewise, the time required for each algorithm to reach the best solution is shown. The GA presents greater efficiency in terms of computation time in four orders of magnitude, with a precision of 1%.

Table 1. Comparison of genetic algorithm (GA) and exhaustive search (reference).

Global solution					
	Generations				
	10	50	100	500	1000
Difference [%]	15.81	23.06	1.06	1.29	1.14

Time [s]	
GA	Exhaustive search
56.130 ± 31.962	388126.600 ± 57869.629

In terms of the GA performance, it is shown in Fig. 1 the fitness values of the solutions change with the generations and the number of new solutions explored in each generation. This helps to figure out if the GA can find new solutions as an indication of more possible evolution. If no new solutions are explored (as presented beyond 50 generations), this is an indication that no further evolution is possible.

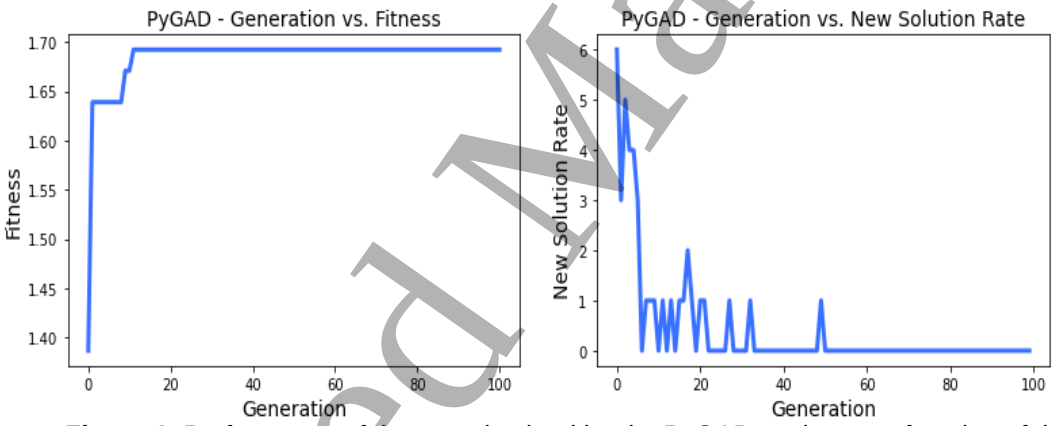

Figure 1. Performance of the genetic algorithm by PyGAD package as function of the generations for a single lesion.

Before performing the optimization, we determine retrospectively the intra-fraction errors by all plans in the 6DOF. It is shown in Table 2 the mean and standard deviation of these shifts. This allows us to establish the 0.2º/0.2 mm criterion.

Table 2. Mean intra-fraction error determined in our institution for single isocenter multiple brain metastases radiosurgery.

Rotation/translation	Intra-fraction error
x [mm]	0.19 ± 0.52
y [mm]	0.21 ± 0.55
z [mm]	0.18 ± 0.57
roll [º]	-0.17 ± 0.36
pitch [º]	0.23 ± 0.42
yaw [º]	0.19 ± 0.54

A positive correlation was observed between the solutions found for the maximum induced error and the distance to the isocenter as shown by the Spearman coefficient (ρ = 0.75 for 0.2º/0.2 mm and ρ = 0.73 for 0.5º/0.5 mm). Fig. 2 shows these values and the linear models.

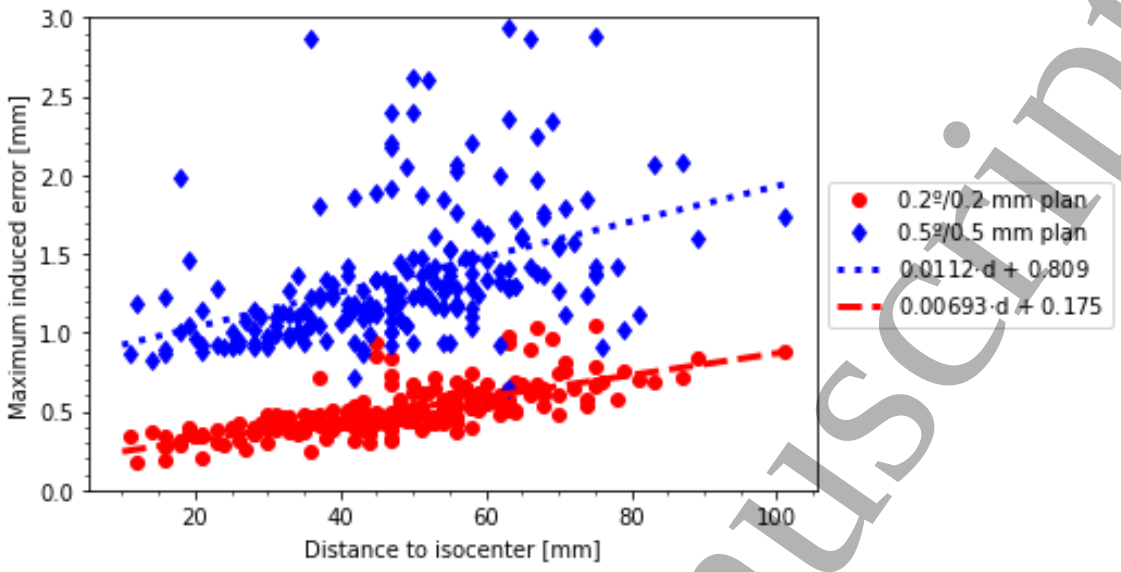

Figure 2. Maximum induced error after applying rotations/translations of 0.5º/0.5 mm, 0.2º/0.2 mm versus the distance from the isocenter. Discontinuos lines are the linear models for each case.

We have to consider that the number of metastases of each plan is a variable that can degrade the quality of a plan. The change in PTV volume for each case is shown in Fig. 3.

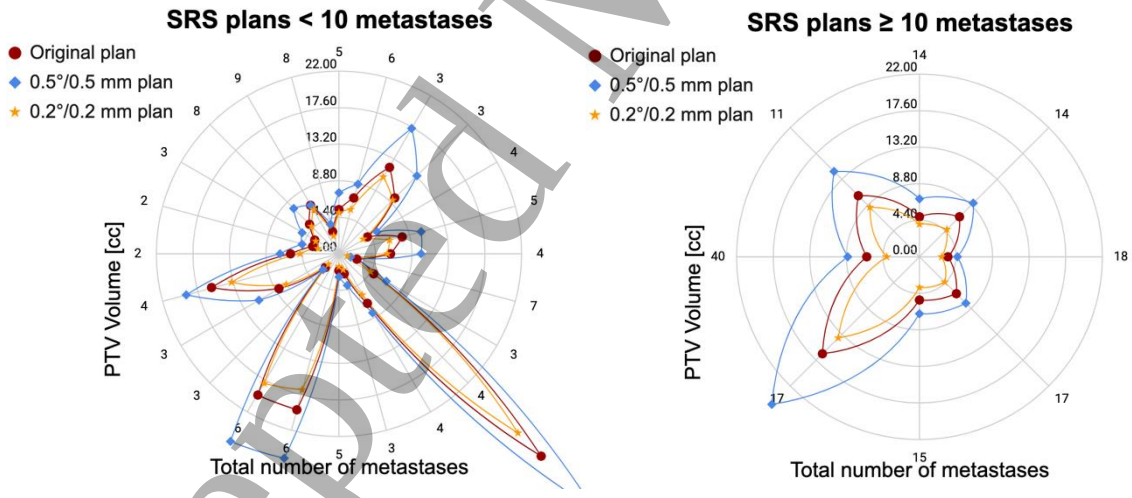

Figure 3. Relation between the number of metastases per plan (polar axis) and the total PTV volume (radial axis) for cases < 10 and ≥ 10 brain metastases applying different criteria to assign margins.

The dosimetric impact was studied through the quality indices for each metastasis. The degradation of the quality indices as a function of the GTV size is shown in Fig. 4. In all cases, the higher the GTV size, the lower the dosimetric variation. The plans with 10 metastases of more show higher dispersion than the plans with a lower number of metastases (differences up to 50%).

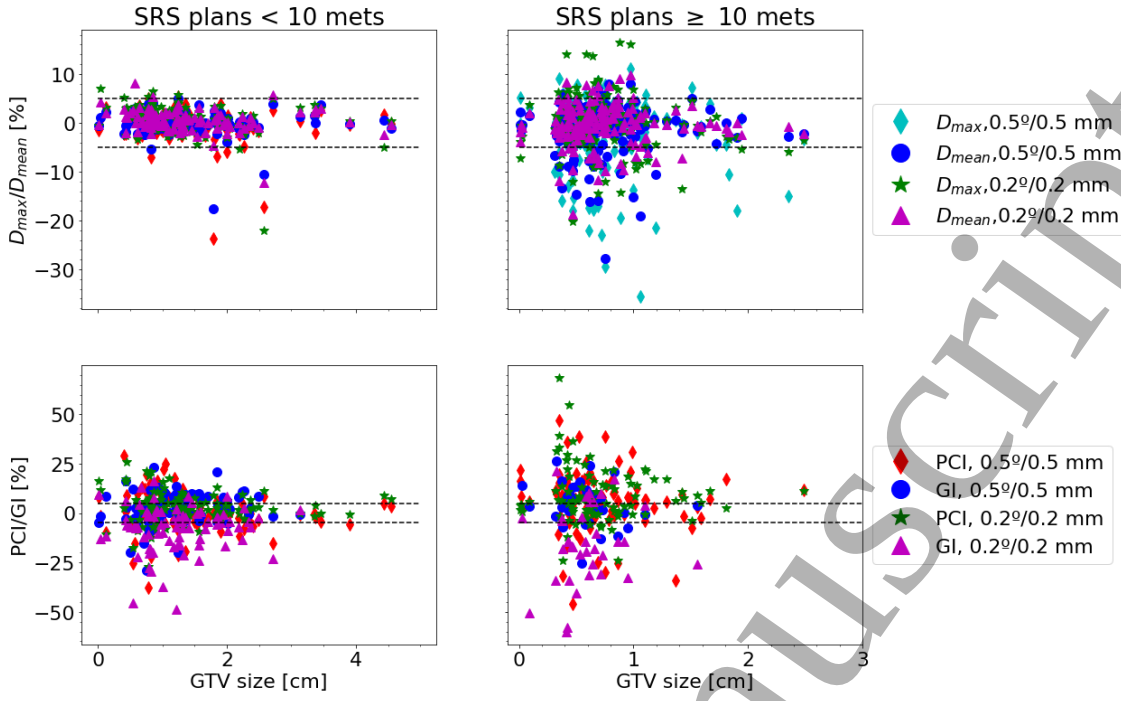

Figure 4. Relative differences of the quality indices as function of GTV size for cases < 10 and ≥ 10 brain metastases applying different criteria to assign margins. Discontinous lines shows the ± 5% range.

There were no statistically significant differences between the optimized-margin plans and the original plans for D_{max}, D_{mean}, and MU. However, considering the 0.5º/0.5 mm plans, PCI and GI decreased for ≥ 10 metastases, and local, and global V_{12} for HB and WB increased considerably in both cases as shown in Table 3. To consider 0.2º/0.2 mm plans, PCI and GI get worse for all cases but local, and global V_{12} for HB and WB decreased in both cases.

Table 3. Dosimetric indices for different plans following original and optimized criteria to assign PTV margins.

Plans < 10 metastases					
Quantity	**Original plan**	**0.5º/0.5 mm plan**	**p-value**	**0.2º/0.2 mm plan**	**p-value**
PTV volume [cc]	8.23 ± 7.52	10.75 ± 9.60	6.9×10^{-6}	7.17 ± 6.74	3.1×10^{-6}
size [cm]	1.40 ± 0.85	1.64 ± 0.87	5.0×10^{-32}	1.46 ± 0.83	4.4×10^{-6}
D_{max} [Gy]	25.42 ± 0.79	25.54 ± 1.41	0.082	25.30 ± 1.40	0.090
D_{mean} [Gy]	23.41 ± 0.49	23.43 ± 0.78	0.356	23.12 ± 2.08	0.072
PCI	0.82 ± 0.06	0.81 ± 0.07	0.254	0.79 ± 0.07	1.1×10^{-5}
GI	4.41 ± 1.09	4.33 ± 1.19	0.061	4.81 ± 1.49	1.5×10^{-7}
local V_{12} [cc]	14.23 ± 12.24	17.64 ± 13.16	0.010	12.19 ± 11.62	0.034
global V_{12} HB [cc]	17.69 ± 13.79	22.25 ± 16.70	1.8×10^{-6}	14.96 ± 13.09	5.8×10^{-6}
global V_{12} WB [cc]	21.04 ± 15.79	27.80 ± 21.97	4.4×10^{-6}	20.51 ± 18.27	0.307
global V_{10} HB [cc]	25.37 ± 20.55	31.94 ± 24.08	7.1×10^{-5}	22.02 ± 19.49	3.9×10^{-6}
global V_{10} WB [cc]	28.59 ± 22.72	37.05 ± 29.88	2.4×10^{-6}	27.66 ± 24.35	0.166
global V_5 HB [cc]	95.47 ± 81.29	119.18 ± 94.38	2.2×10^{-5}	84.72 ± 67.52	0.021
global V_5 WB [cc]	97.39 ± 82.73	126.28 ± 100.94	4.5×10^{-5}	89.29 ± 74.06	0.058
MU	7929 ± 2390	8147 ± 2636	0.174	7754 ± 2094	0.099
Plans ≥ 10 metastases					
Quantity	**Original plan**	**0.5º/0.5 mm plan**	**p-value**	**0.2º/0.2 mm plan**	**p-value**
PTV volume [cc]	7.48 ± 4.19	10.47 ± 6.58	0.005	5.69 ± 3.67	1.1×10^{-4}
Size [cm]	0.75 ± 0.42	1.05 ± 0.44	1.4×10^{-68}	0.88 ± 0.40	1.3×10^{-27}
D_{max} [Gy]	25.96 ± 1.68	26.75 ± 3.04	3.4×10^{-6}	25.96 ± 1.78	0.498

D_{mean} [Gy]	23.63 ± 0.81	24.03 ± 1.57	1.1×10^{-4}	23.72 ± 1.10	0.140
PCI	0.73 ± 0.12	0.68 ± 0.13	9.5×10^{-6}	0.66 ± 0.15	6.5×10^{-9}
GI	6.40 ± 1.29	6.07 ± 1.28	0.004	7.44 ± 2.16	4.2×10^{-5}
local V_{12} [cc]	34.18 ± 33.77	50.59 ± 50.53	0.021	27.89 ± 24.16	0.038
global V_{12} HB [cc]	39.81 ± 30.63	59.10 ± 48.00	0.010	34.13 ± 29.58	0.010
global V_{12} WB [cc]	42.27 ± 30.64	63.44 ± 49.72	0.009	37.82 ± 30.35	0.025
global V_{10} HB [cc]	69.75 ± 66.43	102.28 ± 95.62	0.012	61.95 ± 62.33	0.014
global V_{10} WB [cc]	75.18 ± 66.62	109.62 ± 98.76	0.014	63.97 ± 62.18	0.020
global V_5 HB [cc]	390.89 ± 280.95	460.25 ± 244.77	0.003	345.05 ± 266.11	0.029
global V_5 WB [cc]	393.57 ± 289.28	467.77 ± 245.83	0.005	345.73 ± 266.02	0.025
UM	18101 ± 8190	17482 ± 4862	0.330	18407 ± 7402	0.289

In terms of the healthy tissue, the indices are presented in Fig. 5 as a function of the GTV volume for plans applying different margin criteria. Local V_{12} could be visualized in Fig. 5 (bottom) as the contribution for each metastasis, and the sum of all local V_{12} contributions are presented in Fig. 5 (top) for the total GTV volume. It is noticeable that local V_{12} shows the lowest values in all cases. Analogously, global V_{12} for WB indicates the highest value.

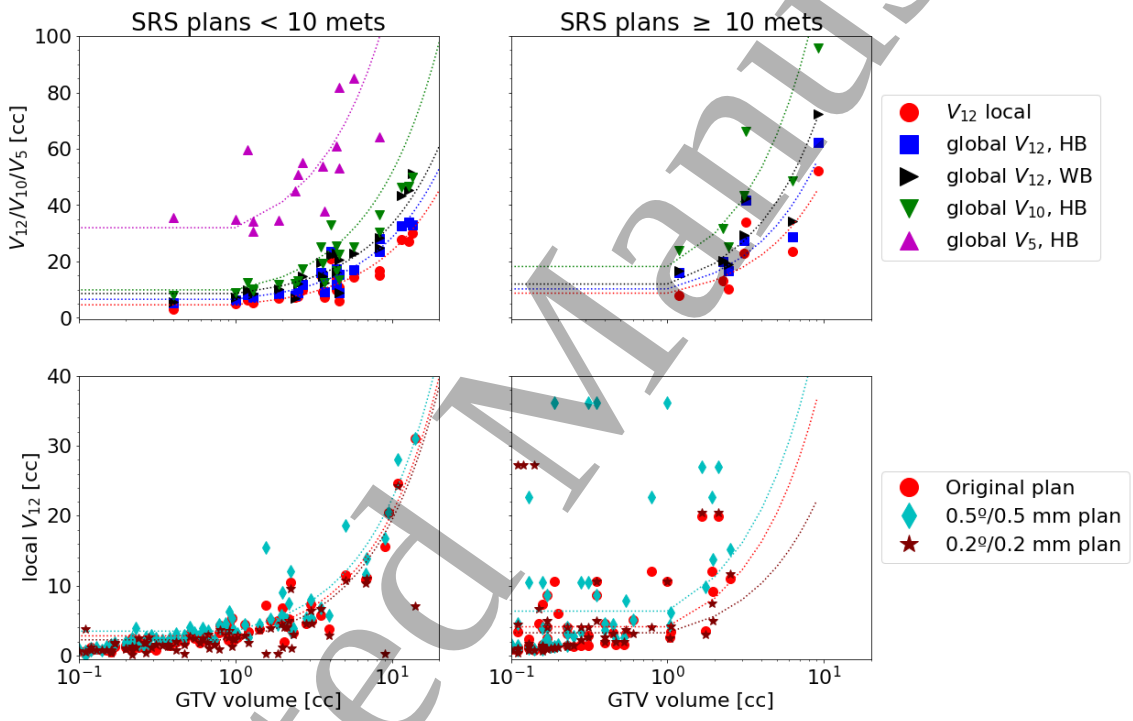

Figure 5. Local and global V_{12}, V_{10} and V_5 for healthy (HB) or whole brain (WB) for plans following original and optimized criteria to assign PTV margins as a function of the total (top) and local (bottom) GTV volume. Discontinuous lines are only for visual guidance.

4. Discussion

Concerning the PTV margin assessment, the use of GA is an effective optimization approach for the determination of maximum induced error, and it seems to be attractive due to its relatively easy implementation as shown in this work.

The justification of the implementation of metaheuristic algorithms based on the space of solutions exhibited here could be simplistic, but the exhaustive search shows that acceptable solutions (with an uncertainty of 1%) can be achieved by GA in few generations, reducing considerably the computation time, allowing to achieve acceptable times in the clinic for analysis of cases with a large number of metastases and to take

into account mechanical constraints during the treatment. In this way, the use of metaheuristic algorithms is a reasonable decision instead of an exhaustive search approach, due to one major practical drawback is its space complexity, as it stores all generated nodes in memory. GA can reduce the use of memory removal in each generation of the non-optimized solutions. Another relevant feature to reach these results is to perform good tuning for the parameters of the GA and to ensure the proper software quality and development process in Python.

At present, there are efforts in the clinical community to evaluate SIMM-SRS the impact of the accuracy to determine targets for geometric variables such as the distance to the isocenter[45], including experimental validation that IGRT positioning accuracy has nothing to do with the distance to the isocenter[46]. However, it is important to take these recommendations carefully, due to before its clinical use, IGRT linac-independent systems such as ExacTrac™ have to be calibrated with the help of tests that determines the accuracy between the mechanical and radiation isocenter, such as the Winston Lutz test (WL). At present, the WL test is performed routinely at the isocenter, but recent publications have started to show relevant shifts of the targets versus the distance to isocenter[45,47]. In these analyses, it is mentioned that the use of the single-isocenter technique to treat multiple lesions is efficient and accurate only when the maximum distance from the center of the mechanical field to the machine isocenter is within 3 cm[47]. So, it is necessary to consider this effect on off-axis targets due to the deviations shown and its impact on dose delivery.

Moreover, in single fraction treatments, the intra-fraction errors produced an uncertainty that has to be considered. In our clinic, we determined that these errors are, on average, 0.2 mm for translations and 0.2º for rotations, corresponding with previous work[27]. These tolerances could be used to determine the maximum induced error that could occur during treatment as a result of a combination of movements. The problem associated with these shifts is mainly that rotations are not rigid transformations, thus the order in which they are applied in combination with translations does matter, as shown in the mathematical description in Appendix.

The use of individualized margins that take into account more sources of uncertainties can provide tools that ensure the correct delivery of doses in brain metastases. However, it should be considered that using wider margins improves quality indices, but increases the risk of necrosis[43] by increasing indicators such as V_{12}. The PTV coverage applying translations and rotations was studied and it was shown that dosimetric changes[48] and tumor control[49] followed a complex function of the displacement's combination. This effect may be related to a previous computational work where it was shown that applying rotations in diverse combinations showed different final displacements[16]. It was related to the rotations being non-rigid transformations, as shown in the Appendix. In this way, the distance to the isocenter is not the only parameter that must be considered for margin assignment, as seen in the displacements produced in Fig. 2. The use of margins that are based on shifts of 0.2º/0.2 mm allows for reducing the volume of HB that is irradiated for plans no matter the number of metastases, with the disadvantage of reducing (not substantially) the quality indices, as shown in Fig. 4 and Table 3.

To reduce variability in the HB contouring, recommendations, as reported in a study[11] were followed to evaluate the risk of brain necrosis, excluding certain structures in the dosimetric evaluation such as the brainstem and GTVs. This analysis presented shows that V_{12} varies regarding if it is local, or global and if the evaluation is for WB or HB. Concerning the protection of the HB, this study agreed with one analysis, indicating that regarding the correlation between the number of metastases and volumes, considering the greater the number of metastases, the more areas of the brain are involved in planning making it more difficult to spare the normal brain[50]. This is noticeable on the

higher dispersion of local V_{12} for GTV volume shown in Fig. 5. This could be related to the fact that there is more probability of dose cluster formation increasing the number of metastases. The effect of the assessment of individualized margins in relation to the dose clusters, produced by the proximity of the lesions, will be study in future work.

In recent years, SIMM-SRS has been performed to treat an increasing number of brain metastases and minimize the negative impacts on quality of life and neurocognition[51]. However, guidelines regarding the number of metastases that can be safely treated are lacking, and practice patterns vary widely[51]. One recent analysis suggests acceptable safety associated with the administration of SRS to ≤15 metastases[52]. In this work, we present the potential use of individualized margins without the increase of damage to healthy brain. It is also presented that for plans with a greater number of metastases, the quality indices play more complex roles as a function of geometric variables. Thus, the analysis associated with the dosimetric impact of these margins invites the development of communication and interaction between medical physicists and radiation oncologists to define the compromise between dose coverage and the protection of normal tissue.

From these considerations, it sounds attractive the use of neural networks in SRS that offers new solutions in reduced times for the PTV margin assignation of multiple brain metastases. The geometric information such as volume, distance to isocenter, relative position in the skull, the total number of metastases per plan, dose cluster formation, and the protection of healthy brain could be included as input to a neural network to classify as output the PTV margins.

5. Limitations

The observable results of this study are based on an isotropic margin approach for SIMM-SRS plans by DCA. The development of adaptative margins as a function of their relative (angular) position to the isocenter and irregular-shape lesions were not covered at the moment.

6. Conclusions

The implementation of a genetic algorithm for the calculation of intra-fractional setup errors in SIMM-SRS is easy, fresh, and not time-consuming in comparison with other strategies such as exhaustive search. This computational approach takes into account more SRS sources of uncertainty, enabling the protection of the healthy brain by “smartly” reducing the margins, and maintaining clinically acceptable PTV coverage in most cases.

In plans that have a large number of metastases or present dose cluster formation due to the fact that the individual metastases are close, the dosimetric variations are greater and require careful review, so the use of a supervised learning model that considers these variables and the genetic algorithm will have a potential advantage to assign margins to lesions considering a greater number of physical and geometric parameters.

7. References

1. Karlsson B, Hanssens P, Wolff R, Söderman M, Lindquist C, Beute G. Thirty years’ experience with Gamma Knife surgery for metastases to the brain. *J Neurosurgery*. 2009;111: 449-457. doi: 10.3171/2008.10.JNS08214.

2. Nichol A, Ma R, Hsu F, et al. Volumetric radiosurgery for 1 to 10 brain metastases: a multicenter, single-arm, phase 2 study. *Int J Radiat Oncol Biol Phys*. 2016;94:312-321. doi: 10.1016/j.ijrobp.2015.10.017.

3. Huang Y, Chin K, Robbins JR, et al. Radiosurgery of multiple brain metastases with single-isocenter dynamic conformal arcs (SIDCA). *Radiother Oncol*. 2014;112: 128–132. doi: 10.1016/j.radonc.2014.05.009.

4. Ziemer BP, Sanghvi P, Hattangadi-Gluth J, Moore KL. Heuristic knowledge-based planning for single-isocenter stereotactic radiosurgery to multiple brain metastases. *Med Phys.* 2017;44(10): 5001–5009. doi: 10.1002/mp.12479.

5. Gevaert T, Steenbeke F, Pellegri L, et al. Evaluation of a dedicated brain metastases treatment planning optimization for radiosurgery: a new treatment paradigm? *Radiat Oncol*. 2016;11-13. doi: 10.1186/s13014-016-0593-y.

6. Nakano H, Tanabe S, Utsunomiya S, et al. Effect of setup error in the single-isocenter technique on stereotactic radiosurgery for multiple brain metastases. *J Appl Clin Med Phys*. 2020 Dec;21(12): 155-165. doi: 10.1002/acm2.13081.

7. Clark GM, Popple RA, Young PE, Fiveash JB. Feasibility of single-isocenter volumetric modulated arc radiosurgery for treatmentof multiple brain metastases. *Int J Radiat Oncol Biol Phys.* 2010;76(1): 296-302. doi: 10.1016/j.ijrobp.2009.05.029.

8. Nath SK, Lawson JD, Simpson DR, et al. Single-isocenter frame-less intensity-modulated stereotactic radiosurgery for simultaneous treatment of multiple brain metastases: clinical experience. *Int J Radiat Oncol Biol Phys.* 2010;78(1): 91-97. doi: 10.1016/j.ijrobp.2009.07.1726.

9. Riis HL, Zimmermann SJ, Hjelm-Hansen M. Gantry and isocenter displacements of a linear accelerator caused by an add-on micromultileaf collimator. *Med Phys*. 2013;40(3):031707. doi: 10.1118/1.4789921.

10. Selvan KT, Padma G, Revathy MK, Nambi NA, Senthilnathan K, Ramesh P. Dosimetric Effect of Rotational Setup Errors in Single-Isocenter Volumetric-Modulated Arc Therapy of Multiple Brain Metastases. *J Med Phys*. 2019;44(2): 84-90. doi: 10.4103/jmp.JMP_103_18.

11. de Camargo AV, Cao M, da Silva DDCSA, Cunha de Aráujo RL. Evaluation of the correlation between dosimetric, geometric, and technical parameters of radiosurgery planning for multiple brain metastases. *J Appl Clin Med Phys*. 2021;22(8): 83-92. doi: 10.1002/acm2.13326.

12. Winey B, Bussiére M. Geometric and dosimetric uncertainties in intracranial stereotatctic treatments for multiple nonisocentric lesions. *J Appl Clin Med Phys*. 2014;15(3): 122–132. doi: 10.1120/jacmp.v15i3.4668.

13. Garcia MA, Anwar M, Yu Y, et al. Brain metastasis growth on preradiosurgical magnetic resonance imaging. *Pract Radiat Oncol*. 2018;8(6): e369-e376. doi: 10.1016/j.prro.2018.06.004.

14. Calmels L, Blak Nyrup Biancardo S, Sibolt P, et al. Single-isocenter stereotactic non-coplanar arc treatment of 200 patients with brain metastases: multileaf collimator size and setup uncertainties. *Strahlenther Onkol.* 2021. doi: 10.1007/s00066-021-01846-6.

15. Venencia CD, Rojas-López JA, Díaz Moreno RM, Zunino S. Rotational effect and dosimetric impact: HDMLC vs 5mm MLC leaf width in single isocenter multiple metastases radiosurgery with Brainlab ElementsTM. *J Radiot in Pract.* 2022. In press. doi: 10.1017/S1460396922000048.

16. Rojas-López JA, Díaz Moreno RM, Venencia CD. Use of genetic algorithm for PTV optimization in single isocenter multiple metastases radiosurgery treatments with Brainlab Elements™. *Phys Med.* 2021;86: 82–90. doi: 10.1016/j.ejmp.2021.05.031.

17. Usui K, Isobe A, Hara N, et al. Development of a rotational set-up correction device for stereotactic head radiation therapy: a performance evaluation. *J Appl Clin Med Phys* 2019;20(6):206-212. doi: 10.1002/acm2.12616.

18. Dhabaan A, Schreibmann E, Siddigi A, et al. Six degrees of freedom CBCT-based positioning for intracranial targets treated with frameless stereotactic radiosurgery. *J Appl Clin Med Phys*. 2012;13(6):215–25. doi: 10.1120/jacmp.v13i6.3916.

19. Ezzell, GA. The spatial accuracy of two frameless, linear accelerator-based systems for single-isocenter, multitarget cranial radiosurgery. *J Appl Clin Med Phys*. 2017;18(2):37–43. doi: 10.1002/acm2.12044.

20. Zhang M, Zhang Q, Gan H, Li S, Zhou S. Setup uncertainties in linear accelerator based stereotactic radiosurgery and a derivation of the corresponding setup margin for treatment planning. *Phys Med*. 2016;32(2):379–85. doi: 10.1016/j.ejmp.2016.02.002.

21. Kang KM, Chai GY, Jeong BK. Estimation of optimal margin for intrafraction movements during frameless brain radiosurgery. *Med Phys*. 2013;40(5):051716. doi: 10.1118/1.4801912.

22. Sagawa T, Ohira S, Ueda Y, et al. Dosimetric effect of rotational setup errors in stereotactic radiosurgery with HyperArc for single and multiple brain metastases. *J Appl Clin Med Phys*. 2019; 20(10): 84–91. doi: 10.1002/acm2.12716.

23. Kuntz L, Matthis R, Wegner N, Lutz S. Dosimetric comparison of mono-isocentric and multi-isocentric plans for oligobrain metastases: A single institutional experience. *Cancer Radiother*. 2020;24(1): 53–9. doi: 10.1016/j.canrad.2019.10.003.

24. Jhaveri J, Chowdhary M, Zhang X, et al. Does size matter? Investigating the optimal planning target volume margin for postoperative stereotactic radiosurgery to resected brain metastases. *J Neurosurg*. 2018;130(3): 797–803. doi: 10.3171/2017.9.JNS171735.

25. Symposium, Novalis Circle. 2019. *Impact of margins for single isocenter multiple target treatments AAPM 2019*. https://www.novaliscircle.org/video/impact-of-marginsfor-single-isocenter-multiple-target-treatments-dWQSM9a/. Accessed Jan 26, 2022.

26. Roper J, Chanyavanich V, Betzel G, Switchenko J, Dhabaan A. Single-isocenter multiple-target SRS: risk of compromised coverage. *Int J Radiat Oncol. Biol. Phys.* 2015;93(3):540-6. doi: 10.1016/j.ijrobp.2015.07.2262.

27. Minniti G, Capone L, Alongi F, et al., Initial Experience With Single-Isocenter Radiosurgery to Target Multiple Brain Metastases Using an Automated Treatment Planning Software: Clinical Outcomes and Optimal Target Volume Margins Strategy, *Advances in Radiation Oncology*, 2020;5(5): 856-864. doi: 10.1016/j.adro.2020.06.008.

28. Fallahi, A., Mahnam, M., & Niaki, S. T. A. Direct aperture optimization for intensity modulated radiation therapy: Two calibrated metaheuristics and liver cancer case study. *International Journal of Industrial Engineering and Production Research*, 2022; 33(2), 1–14. doi: 10.22068/ijiepr.33.2.4.

29. Fallahi, A., Mahnam, M., & Niaki, S. T. A. A discrete differential evolution with local search particle swarm optimization to direct angle and aperture optimization in IMRT treatment planning problem. *Applied Soft Computing*. 2022. doi: 10.1016/j.asoc.2022.109798

30. Potvin J-Y, Smith KA. *Artificial Neural Networks for Combinatorial Optimization. Handbook of metaheuristics.* Springer; 2003. doi: 10.1007/0-306-48056-5_15.

31. Reeves C. *Genetic Algorithms. Handbook of Metaheuristics. International Series in Operations Research & Management Science*. vol 57. Boston. Springer; 2003. doi: 10.1007/0-306-48056-5_3.

32. Nazareth DP, Brunner S, Jones MD, et al. Optimization of beam angles for intensity modulated radiation therapy treatment planning using genetic algorithm on a distributed computing platform. *J Med Phys*. 2009;34(3):129-132. doi: 10.4103/0971-6203.54845.

33. Yu Y, Schell MC, Zhang JB. Decision theoretic steering and genetic algorithm optimization: application to stereotactic radiosurgery treatment planning. *Med Phys*. 1997;24(11): 1742-1750. doi: 10.1118/1.597951.

34. Chang J. A statistical model for analyzing the rotational error of single isocenter for multiple targets technique. *Med Phys*. 2017;44(6): 2115-2123. doi: 10.1002/mp.12262.

35. Agazaryan N, Tenn S, Lee C, Steinberg M, Hegde J, Chin R, Pouratian N, Yang I, Kim W, Kaprealian T. Simultaneous radiosurgery for multiple brain metastases: technical overview of the UCLA experience. *Radiat Oncol*. 2021;17;16(1):221. doi: 10.1186/s13014-021-01944-w.

36. Vergalasova I, Liu H, Alonso-Basanta M, et al. Multi-Institutional Dosimetric Evaluation of Modern Day Stereotactic Radiosurgery (SRS) Treatment Options for Multiple Brain Metastases. *Front. Oncol.* 2019;7(9):483. doi: 10.3389/fonc.2019.00483.

37. Mohan R, Chui C, Lidofsky L. Energy and angular distributions of photons from medical linear accelerators. *Med Phys.* 1985;12(5): 592–7. doi: 10.1118/1.595680

38. Mohan R, Chui C, Lidofsky L. Differential pencil beam dose computation model for photons. *Med Phys*. 1986;13(1): 64-73. doi: 10.1118/1.595924.

39. Rojas-López JA, Fotinós J, Maddalozzo N, Dicomhandler: Python tool for manipulating DICOM files and its application for radiosurgery. *Software Impacts.* Published March 6, 2023. In press. doi: https://doi.org/10.1016/j.simpa.2023.100487

40. Chen JJ. The Hardy-Weinberg principle and its applications in modern population genetics. *Front. Biol.* 2010;5:348–353. doi: 10.1007/s11515-010-0580-x.

41. Gad AF, PyGAD. https://pygad.readthedocs.io/en/latest/Footer.html#submitting-issues. Accessed Jan 15, 2023.

42. Brainlab. 2020. Brainlab Physics, RT Elements Brainlab Physics. Technical Reference Guide. Germany: Brainlab AG.

43. Milano MT, Grimm J, Niemierko A, Soltys SG, Moiseenko V, Redmond KJ, et al. Single- and Multifraction Stereotactic Radiosurgery Dose/Volume Tolerances of the Brain. *Int J Radiat Oncol Biol Phys*. 2021 May 1;110(1):68-86. doi: 10.1016/j.ijrobp.2020.08.013.

44. Minniti G, Capone L, Nardiello B, El Gawhary R, Raza G, Scaringi C, Bianciardi F, Gentile P, Paolini S. Neurological outcome and memory performance in patients with 10 or more brain metastases treated with frameless linear accelerator (LINAC)-based stereotactic radiosurgery. *J Neurooncol*. 2020 May;148(1):47-55. doi: 10.1007/s11060-020-03442-7.

45. Pudsey LMM, Biasi G, Ralston A, Rosenfeld A, Poder J. Detection of rotational errors in single-isocenter multiple-target radiosurgery: Is a routine off-axis Winston-Lutz test necessary? *J Appl Clin Med Phys*. 2022 Sep;23(9):e13665. doi: 10.1002/acm2.13665.

46. Ahn KH, Yenice KM, et al. Frame-based radiosurgery of multiple metastases using single-isocenter volumetric modulated arc therapy technique. *J Appl Clin Med Phys*. 2019 Aug;20(8):21-28. doi: 10.1002/acm2.12672.

47. Gao J, Liu X. Off-Isocenter Winston-Lutz Test for Stereotactic Radiosurgery/Stereotactic Body Radiotherapy. *International Journal of Medical Physics, Clinical Engineering and Radiation Oncology*. 2016;5:154-161. doi: 10.4236/IJMPCERO.2016.52017.

48. Eder MM, Reiner M, Heinz C, et al. Single-isocenter stereotactic radiosurgery for multiple brain metastases: Impact of patient misalignments on target coverage in non-coplanar treatments. *Z Med Phys*. 2022 Aug;32(3):296-311. doi: 10.1016/j.zemedi.2022.02.005.

49. Palmiero AN, Fabian D, Randall ME, et al. Predicting the effect of indirect cell kill in the treatment of multiple brain metastases via single-isocenter/multitarget volumetric modulated arc therapy stereotactic radiosurgery. *J Appl Clin Med Phys*. 2021 Oct;22(10):94-103. doi: 10.1002/acm2.13400.

50. Becker SJ, Lipson EJ, Jozsef G, Molitoris JK, Silverman JS, Presser J, Kondziolka D. How many brain metastases can be treated with stereotactic radiosurgery before the radiation dose delivered to normal brain tissue rivals that associated with standard whole brain radiotherapy? *J Appl Clin Med Phys*. 2023 Jan 11:e13856. doi: 10.1002/acm2.13856.

51. Sandler KA, Shaverdian N, Cook RR, et al. Treatment trends for patients with brain metastases: does practice reflect the data? *Cancer.* 2017;123(12):2274-2282. doi:10.1002/cncr.30607.

52. Hughes RT, Masters AH, McTyre ER, et al. Initial SRS for patients with 5 to 15 brain metastases: results of a multi-institutional experience. *Int J Radiat Oncol Biol Phys*. 2019;104(5):1091-1098. doi:10.1016/j.ijrobp.2019.03.052.

Appendix

To prove that the order in which the rotations and translations are performed influences the effective shift of a point in space, as well as the fact that applying the translations in a certain order is not equivalent to the fact that they are performed at last in an additive way, let us consider two cases, in which rotations of angle θ and translations of shift Δ are applied.

First, we consider the following transformations for roll $R_{R\theta}$, pitch $R_{P\theta}$ and yaw $R_{Y\theta}$ rotations, as well as x $T_{x\Delta}$, y $T_{y\Delta}$ and z $T_{z\Delta}$ translations. The set of transformations are:

$$R_{R\theta} = \begin{pmatrix} \cos\theta & 0 & \sin\theta & 0 \\ 0 & 1 & 0 & 0 \\ -\sin\theta & 0 & \cos\theta & 0 \\ 0 & 0 & 0 & 1 \end{pmatrix}$$

$$R_{P\theta} = \begin{pmatrix} 1 & 0 & 0 & 0 \\ 0 & \cos\theta & -\sin\theta & 0 \\ 0 & \sin\theta & \cos\theta & 0 \\ 0 & 0 & 0 & 1 \end{pmatrix}$$

$$R_{Y\theta} = \begin{pmatrix} \cos\theta & -\sin\theta & 0 & 0 \\ \sin\theta & \cos\theta & 0 & 0 \\ 0 & 0 & 1 & 0 \\ 0 & 0 & 0 & 1 \end{pmatrix}$$

$$T_{x\Delta} = \begin{pmatrix} 1 & 0 & 0 & \Delta \\ 0 & 1 & 0 & 0 \\ 0 & 0 & 1 & 0 \\ 0 & 0 & 0 & 1 \end{pmatrix}$$

$$T_{y\Delta} = \begin{pmatrix} 1 & 0 & 0 & 0 \\ 0 & 1 & 0 & \Delta \\ 0 & 0 & 1 & 0 \\ 0 & 0 & 0 & 1 \end{pmatrix}$$

$$T_{z\Delta} = \begin{pmatrix} 1 & 0 & 0 & 0 \\ 0 & 1 & 0 & 0 \\ 0 & 0 & 1 & \Delta \\ 0 & 0 & 0 & 1 \end{pmatrix}.$$

First let us study the case of $R_{R\theta}T_{x\Delta}R_{P\theta}T_{y\Delta}R_{Y\theta}T_{z\Delta}$. If we apply the above transformations, we obtain

$$R_{R\theta}T_{x\Delta}R_{P\theta}T_{y\Delta}R_{Y\theta}T_{z\Delta} = \begin{pmatrix} \cos^2\theta + \sin^3\theta & \sin^2\theta\cos\theta - \sin\theta\cos\theta & \sin\theta\cos\theta & \Delta(\sin\theta\cos\theta + \sin^2\theta + \cos\theta) \\ \sin\theta\cos\theta & \cos^2\theta & -\sin\theta & -\Delta(\sin\theta + \cos\theta) \\ \sin^2\theta\cos\theta - \sin\theta\cos\theta & \sin^2\theta + \sin\theta\cos^2\theta & \cos^2\theta & \Delta(\cos^2\theta + \sin\theta\cos\theta - \sin\theta) \\ 0 & 0 & 0 & 1 \end{pmatrix}.$$

If we consider the small angle approximation, then:

$$R_{R\theta}T_{x\Delta}R_{P\theta}T_{y\Delta}R_{Y\theta}T_{z\Delta} = \begin{pmatrix} \theta^3 + 1 & \theta(\theta - 1) & \theta & \Delta(\theta^2 + \theta + 1) \\ \theta & 1 & -\theta & -\Delta(1 - \theta) \\ \theta(\theta - 1) & \theta(\theta + 1) & 1 & \Delta \\ 0 & 0 & 0 & 1 \end{pmatrix}.$$

Finally, if we consider that this transformation is applied to a point $P = (u, v, w, 1)$ from the isocenter, then, the shift experimented by this point before (P) and after (P') the rotation/translation movement is measured as:

$$dist(P' - P) = \left\| \left(R_{R\theta}T_{x\Delta}R_{P\theta}T_{y\Delta}R_{Y\theta}T_{z\Delta} - 1\right)P^T \right\| = \sqrt[2]{\theta^2(\theta^4 + \theta^2 - 2\theta + 6) + \Delta^2(\theta^4 + 2\theta^3 + 4\theta^2 + 3)}.$$

In a similar way, we deduce the description of the shift of a point, given a different order of rotations/translations such as the case of $R_{R\theta}R_{P\theta}R_{Y\theta}T_{x\Delta}T_{y\Delta}T_{z\Delta}$, thus:

$$R_{R\theta}R_{P\theta}R_{Y\theta}T_{x\Delta}T_{y\Delta}T_{z\Delta}$$
$$= \begin{pmatrix} \cos^2\theta + \sin^3\theta & \sin^2\theta\cos\theta - \sin\theta\cos\theta & \sin\theta\cos\theta & \Delta(\cos^2\theta + \sin^3\theta + \sin^2\theta\cos\theta) \\ \sin\theta\cos\theta & -2\sin\theta\cos\theta & -\sin\theta & -\Delta(\sin\theta\cos\theta + \sin\theta) \\ \sin^2\theta\cos\theta - \sin\theta\cos\theta & \sin^2\theta + \sin\theta\cos^2\theta & \cos^2\theta & \Delta(\sin^2\theta\cos\theta + \sin\theta\cos^2\theta - \sin\theta\cos\theta + 1) \\ 0 & 0 & 0 & 1 \end{pmatrix}.$$

If we consider the small angle approximation, then:

$$R_{R\theta}R_{P\theta}R_{Y\theta}T_{x\Delta}T_{y\Delta}T_{z\Delta} = \begin{pmatrix} \theta^3 + 1 & \theta(\theta-1) & \theta & \Delta\left(\theta^3 + \theta^2 + 1\right) \\ \theta & -2\theta & -\theta & -\Delta(1-\theta) \\ \theta(\theta-1) & \theta(\theta+1) & 1 & \Delta\left(\theta^2 - \theta + 2\right) \\ 0 & 0 & 0 & 1 \end{pmatrix}.$$

Finally, if we consider that this transformation is applied to the point P from the isocenter, then, the shift experimented by this point before and after the rotation/translation movement is measured as:

$$dist(P' - P) = \left\|\left(R_{R\theta}R_{P\theta}R_{Y\theta}T_{x\Delta}T_{y\Delta}T_{z\Delta} - 1\right)P^T\right\|$$
$$= \sqrt[2]{(\theta^6 + 3\theta^4 - 2\theta^3 + 2\theta^2 - 4\theta - 1) + \Delta^2(\theta^6 + 2\theta^5 + 2\theta^4 + 9\theta^2 - 2\theta + 6)}.$$

Evidently, but transformations are different in the general case and in the small angle approximation. This difference is represented in the nonequivalent Euclidean distances in both cases.